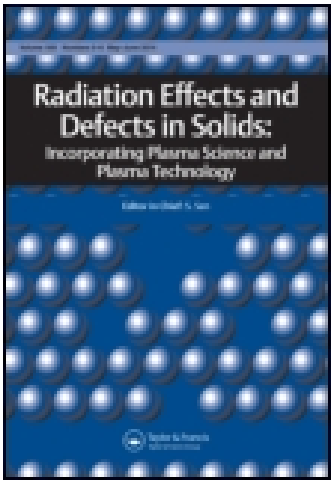

Radiation Effects and Defects in Solids: Incorporating Plasma Science and Plasma Technology
Publication details, including instructions for authors and subscription information:
http://www.tandfonline.com/loi/grad20

Global evaluation of coronal heating due to magnetic reconnection based on solar dynamics observatory observations

J.C. Burke[a] & J.J. Martinell[a]
[a] Instituto de Ciencias Nucleares, Universidad Nacional Autónoma de México, A. Postal 70-543, México D.F., Mexico
Published online: 10 Feb 2015.

To cite this article: J.C. Burke & J.J. Martinell (2015) Global evaluation of coronal heating due to magnetic reconnection based on solar dynamics observatory observations, Radiation Effects and Defects in Solids: Incorporating Plasma Science and Plasma Technology, 170:2, 91-102, DOI: 10.1080/10420150.2014.993636

To link to this article: http://dx.doi.org/10.1080/10420150.2014.993636

Radiation Effects & Defects in Solids, 2015
Vol. 170, No. 2, 91–102, http://dx.doi.org/10.1080/10420150.2014.993636

Global evaluation of coronal heating due to magnetic reconnection based on solar dynamics observatory observations

J.C. Burke and J.J. Martinell*

Instituto de Ciencias Nucleares, Universidad Nacional Autónoma de México, A. Postal 70-543, México D.F., Mexico

(*Received 23 August 2014; final version received 27 November 2014*)

The energy flux released into the corona is estimated from magnetic reconnection events in all spatial scales, covering down to nanoflares. The reconnection model used is based on a quasi-3D configuration that approximates the braiding of magnetic field lines which is produced by photospheric motions and includes both resistive and collisionless reconnection, depending on the event size [Martinell, J.J. *Rad. Effects Defec. Solids* **2010**, *165*, 114]. This model is applied to all length scales involved in the energy release adding all them up. In order to obtain the size distribution, the observations of the *Solar Dynamics Observatory* (*SDO*) are used for two wavelengths in the far UV, together with the corresponding magnetograms and look for correlations brightness-magnetic field. Since the resolution limit of the *SDO* is just above the nanoflare scales, the spectral index of the energy distribution is determined and it is used to extrapolate down to nanoflare scales. An upper limit of the energy flux is obtained following two different methods, as well as an estimate for the aspect ratio of the current sheets. The energy flux estimates are in the range of 300 $\mathrm{W/m^2}$ which is of the order needed to maintain the hot corona.

Keywords: magnetic reconnection; magnetic fields; coronal heating

1. Introduction

Ever since it was discovered that the solar corona has a temperature of the order of 2×10^6 K, the problem of how the corona is heated has received a great deal of attention. Two mechanisms have been considered as the most likely to deliver non-thermal energy to the upper solar atmosphere (*1*, *2*). In both cases the energy in the convection region is the source that feeds the corona with the required thermal energy, and the presence of the magnetic fields is required for the mechanisms to operate. One possibility is that the subphotospheric motions generate magnetohydrodynamic (MHD) waves which propagate upwards along the magnetic field lines, and when they reach the corona the waves are dissipated, producing heat. It has been determined that the compressional waves do not carry the energy required to maintain the hot corona, so that the type of waves that can transport the energy are transverse Alfvén waves. The dissipation can be due to resonant absorption or the result of phase mixing of different waves. These processes require the magnetic flux tubes that support the wave propagation to have a transverse gradient

*Corresponding author. Email: martinel@nucleares.unam.mx

with a characteristic scale length which has to be small enough for the dissipation to be efficient. Recently, observational evidence in favor of Alfvén wave heating has been reported by McIntosh et al. (*3*) and by Tomczyl et al. (*4*), who claim that the energy carried by the waves in the corona is high enough to account for the actual coronal temperature. Although the waves reportedly carry a large amount of energy, the question about the dissipation efficiency still remains to be answered.

The second mechanism arises as the photospheric foot-points of the magnetic field lines slowly move and produce the magnetic field lines in the corona to get twisted, thus accumulating energy in different magnetic structures such as tangential discontinuities (appearing at magnetic surface boundaries when there is magnetic braiding) or current sheets (CSs). This magnetic energy can then be released via magnetic reconnection at the sites where the field becomes more stressed. This process should be taking place at multiple scale lengths, and the number of events at each scale should increase as the scale length becomes smaller, while the energy decreases. Thus, energy-releasing events with energies billionths of times weaker than the energy in an ordinary solar flare could be so numerous that can provide most of the energy to heat the corona. These are the nanoflare events postulated by Parker (*5*) as the main processes that dissipate the accumulated magnetic stresses. However, not enough evidence has been obtained for any of the two mechanisms and a combination of both is likely to occur.

In this work we consider multi-scale flares (down to the nanoflare scale) as the source of coronal heating and make an estimate of the energy flux they can input into the corona based on the reconnection model and on the observations of the coronal emissions recorded by the *Atmospheric Imaging Assembly* (*AIA*) of the *Solar Dynamics Observatory* (*SDO*). Our working hypothesis is that the radiation emission from the upper atmosphere is related to the occurrence of some reconnection events that release energy accumulated by magnetic flux rope braiding or an equivalent process that produces magnetic null points. Compared with the value required to explain the observed temperature, which is around $300\,\mathrm{W/m^2}$, our estimate turns out to be of the same order of magnitude albeit in the lower side. However, the difference can be accounted for by the contribution from scales below the resolution limit in the images. This extra contribution can be included in the estimate by using the energy spectrum inferred from the observed distribution of events and extrapolating to smaller scales. Direct evidence of magnetic reconnection in a solar flare has just been provided by Su et al. (*6*) using high-resolution images from *AIA*, showing there is heated plasma coming out of the flare region. One would expect that this same process should be acting in all scales down to the nano-flare events.

We start the study with a presentation, in Section 2, of the mathematical reconnection model used to estimate the reconnection rate as function of the scale length. Then Section 3 is devoted to analyzing the *AIA* images at two wavelengths in order to determine the emission distribution over the full solar disk at a given time. Together with magnetometer data of the photosphere from the Helioseismic and Magnetometer Imager (HMI) instrument, this information is used to determine the regions of possible reconnection events. Then, based on the previous analyses, an estimate of an upper limit for the released magnetic energy is presented in Section 4; an estimate of the reconnection current sheet width is also obtained. Finally, in Section 5 we discuss the results of our study and the conclusions are drawn.

2. Reconnection model

In order to estimate the power released in a reconnection event we use a two fluid model to describe de plasma, in a geometry that approximately describes the magnetic field line braiding. When a magnetic flux tube is twisted by the motion of the footpoints anchored at the photosphere, the magnetic field lines which are initially, in the ideal case, smooth loops extending to the corona, are braided and the magnetic field lines become sheared. The shear is related to the

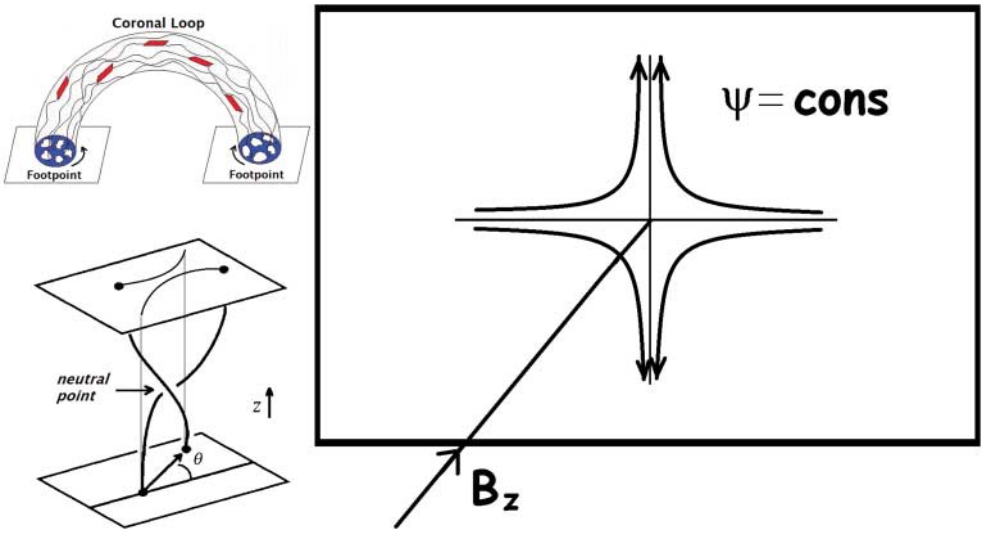

Figure 1. Magnetic field geometry: top left, coronal magnetic loop twisted from the photospheric footpoints (blue) developing local CSs (red); bottom left, straight-cylinder representation of a section of the magnetic loop with the twisted magnetic field around a local neutral point; right, approximated geometry with a guide field along z and an X-point field in the x–y plane.

presence of electrical currents that add another component to the initial magnetic field of the loops. At certain points the currents may be very localized forming CSs aligned with the original field, so that there are no points of vanishing magnetic field, as illustrated in Figure 1. This can be described by a 3D magnetic field consisting of a 2D component with a magnetic X-point in a plane and a perpendicular guide field: $\mathbf{B} = \hat{z} \times \nabla\psi(x,y,t) + B_z(x,y,t)\hat{z}$ with ψ being the magnetic flux function. This represents the field locally around a reconnection region and thus the guide field B_z, representing the initial field of the loop, is taken as constant. The braiding is given by the flux function ψ, which is initially taken here as an X-point configuration $\psi(x,y,t=0) = \psi_0(x,y) = B'_\perp xy$, as shown in Figure 1. In this frame of reference the plasma enters toward the X-point from two opposite directions, thus driving the reconnection in the xy plane.

The relevant fluid equations are the continuity equation and the electron and ion momentum equations, which can be reduced to a three-field model for ψ, the ion stream function ϕ (defined through $\mathbf{v}_i = \hat{z} \times \nabla\phi$) and the density $n = n_e = n_i$. The reduced equations are derived in (*7*, *8*). They include the two regimes of resistive and collisionless plasmas, thus allowing both processes of reconnection to be considered in the model. These equations are applicable to the strong guide field ordering, $\beta < 1$ and for the case $\ell_0/d_i \gg 1$, where $d_i = c/\omega_{pi}$ is the ion skin depth and $\ell_0 = B_{z0}/B'_\perp$ is the relative magnetic field scale length, which are appropriate for the conditions in the solar corona. In addition, the equations are valid in the important regime $\rho_s > d_e$, prevailing in the lower corona, since for typical parameters the ion-sound gyroradius is $\rho_s \approx 50\,\text{cm}$ while the electron skin depth is $d_e \approx 5\,\text{cm}$. The full model is described in (*9*). The set of equations is

$$\frac{\partial U}{\partial t} = [U,\phi] + [\psi,\nabla^2\psi], \tag{1}$$

$$\frac{\partial}{\partial t}(\psi - d_e^2\nabla^2\psi) = [\psi - d_e^2\nabla^2\psi,\phi] - \rho_s^2[\psi,\xi] + \epsilon_\eta\nabla^2\psi, \tag{2}$$

$$\frac{\partial \xi}{\partial t} = [\xi,\phi] + [\psi,\nabla^2\psi], \tag{3}$$

where $[f,g] \equiv \hat{z}\cdot\nabla f\times\nabla g$, $U\equiv\nabla^2\phi$ is the vorticity and $\xi\equiv(\ell_0/d_\mathrm{i})\log(n/n_0)$. All quantities are normalized to the characteristic values in the reconnection region, thus the same model applies for all scales. In addition to the resistive diffusion term, ϵ_η in Equation (2), the collisionless terms due to electron inertia, $d_\mathrm{e}=c/\omega_\mathrm{pe}$, and parallel compressibility, $\rho_\mathrm{s}=v_\mathrm{s}/\Omega_\mathrm{ci}$, can contribute to reconnection. Notice that the equations are not linearized, so that the full nonlinear evolution can be followed. These equations are solved in a squared domain of size $2L$ using a trapezoidal leap-frog scheme, starting from the initial state $\psi_0(x,y)$ for a given set of parameters, namely, the plasma velocity into the X-point, v_0, ϵ_η, ρ_s and d_e. Depending on the plasma conditions at the reconnecting region, the value of the collision mean-free path (λ_c) relative to the reconnection scale length L, determines if the process is either collisional ($\lambda_\mathrm{c}<L$) or collisionless ($\lambda_\mathrm{c}>L$).

Following the same procedure used by Martinell (*9*) to solve numerically Equations (1)–(3), the time evolution of the system is obtained, when the plasma flow is driven from the boundaries by imposing an inwards velocity, v_0. In terms of the steam function, the initial and boundary conditions are

$$\phi(x,y)|_{t=0}=\frac{v_0\ell_0}{4}\ln\left(\frac{y^2+\epsilon^2}{x^2+\epsilon^2}\right),\quad \phi\left(\begin{pmatrix}|x|\\|y|\end{pmatrix}=L,t\right)=\pm\frac{f(t)}{4}\ln\left(\begin{pmatrix}y\\x\end{pmatrix}^2+\epsilon^2\right),\quad (4)$$

where ϵ is a parameter of the order of ρ_s used to avoid singularities and the forcing function $f(t)=v_0\ell_0(1-\exp(-t/\tau_d))$, provides an asymptotically steady drive. The time evolution shows that the field lines coming towards the X-point reconnect and move away from it; when the forcing velocity is large enough the X-point evolves to a CS. The normalized reconnected flux is measured by $\hat{\psi}(x=y=0,t)=\psi(x=y=0,t)/(\delta^2B'_\perp)$ from which the corresponding reconnection rate $\dot{\hat{\psi}}=\mathrm{d}\hat{\psi}(x=y=0)/\mathrm{d}t$ is obtained. For each collisional regime, there is a characteristic value of the reconnection rate obtained for the typical (normalized) parameters of coronal regions, that is, $\rho_\mathrm{s}^2=0.1$, $d_\mathrm{e}^2=10^{-3}$, in a collisionless plasma and $\epsilon_\eta=10^{-2}$ in the resistive case. Figure 2(a) shows $\dot{\hat{\psi}}$ as a function of time for a collisional plasma and it is seen that after a few Alfvén times it settles to an asymptotic value. For the appropriate parameters, using for v_0 the velocity of the foot points, which according to (*1*) is $\approx 10^5$ cm/s, the rate is found to be $\dot{\hat{\psi}}_\mathrm{c}=1.1\times10^{-3}$. Similarly, Figure 2(b) gives $\dot{\hat{\psi}}$ for a non-collisional regime, showing also

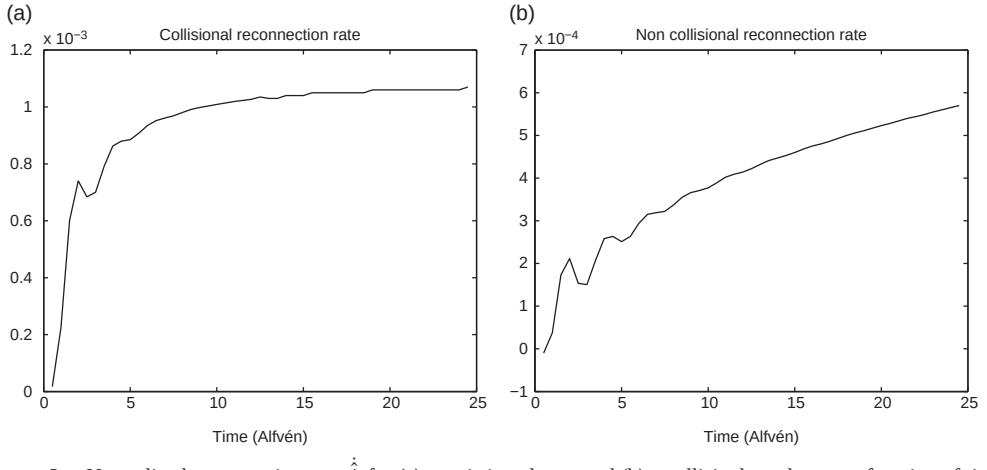

Figure 2. Normalized reconnection rate $\dot{\hat{\psi}}$ for (a) a resistive plasma and (b) a collisionless plasma as function of time in units of the Alfvén time $\tau_\mathrm{A}=(4\pi n_0 m_\mathrm{i})^{1/2}/B'_\perp$.

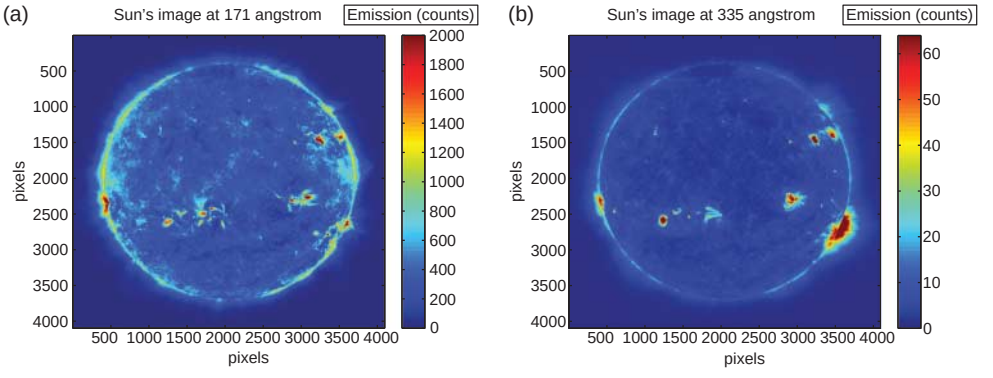

Figure 3. *SDO* images for (a) 17.1 nm and (b) 33.5 nm.

the approach to an asymptotic value although at a slower pace. For this regime the reconnection rate is also lower $\dot{\hat{\psi}}_{\rm nc} = 6 \times 10^{-4}$. These values are used for the heating model developed later.

3. Observational data

The information about the distribution of events is obtained from the high-resolution pictures of the *AIA* instrument in the *SDO*, having 4096×4096 pixels. Each pixel amounts to about 0.6 arcsec or 440 km. The wavelengths chosen are 335 Å (Fe XVI) and 171 Å (Fe IX) corresponding to the active corona and the quiet corona/transition region, respectively. Our hypothesis is that, at any time, the corona is being heated by magnetic field dissipation at all scales and therefore we can use solar images at any desired time to obtain a representative average estimate of the heating. The images chosen here are from the date 12/25/2010 and time 13:36:00, and are shown in Figure 3 for the two wavelengths. In addition to the coronal emissions, the photospheric magnetic fields are obtained from the magnetogram given by the HMI instrument for the same day and time, with approximately the same resolution; the observations for this image are made in the visible line 6173 Å (Fe I). The full magnetogram is shown in Figure 4, but it appears rotated with respect to the UV images of Figure 3 and slightly larger. Since these correspond to photospheric fields they have to be extrapolated up to the corona.

The estimation of the strength of the coronal fields is not unique since it depends on the altitude of the event, which is not known. At the base of the corona, the magnetic measurements reported by Bogod and Yasnov (*10*) for two active regions indicate that there is a reduction from its photospheric value by a factor of 0.3–0.4; on the other hand, measurements for heights of the order of $1R_\odot$ give magnetic field magnitudes on the order of 1 G (*11*), which is about one thousandth of the value at the photosphere. Thus, a flare event could occur at any altitude with typical field magnitude between 1 G and 600 G. In order to have an 'average' value we choose the field strength at 0.05 $R_\odot$, given by the active region magnetic field model $B(R) = 0.5/(R/R_\odot - 1)^{1.5}$ G (*12*) which gives 40 G. This represents a reduction of $\frac{40}{1000} = 0.04$ from photospheric values. So we use this reduction factor all over the regions to get the magnitude of the coronal magnetic field from the photospheric field, assuming it is applicable to quiet and active regions alike. The reduction factor obtained for 0.05 $R_\odot$ is assumed to apply, on average, for higher altitudes, which can be justified on the basis that for twisted magnetic flux tubes, the divergence of field lines with height is very small as shown by Robertson et al. (*13*); they even found that the field amplitude increases with twisting angle.

The main assumption in this work is that the contributions to the coronal heating can be obtained from the emission maps, by taking those bright regions that also have a high value

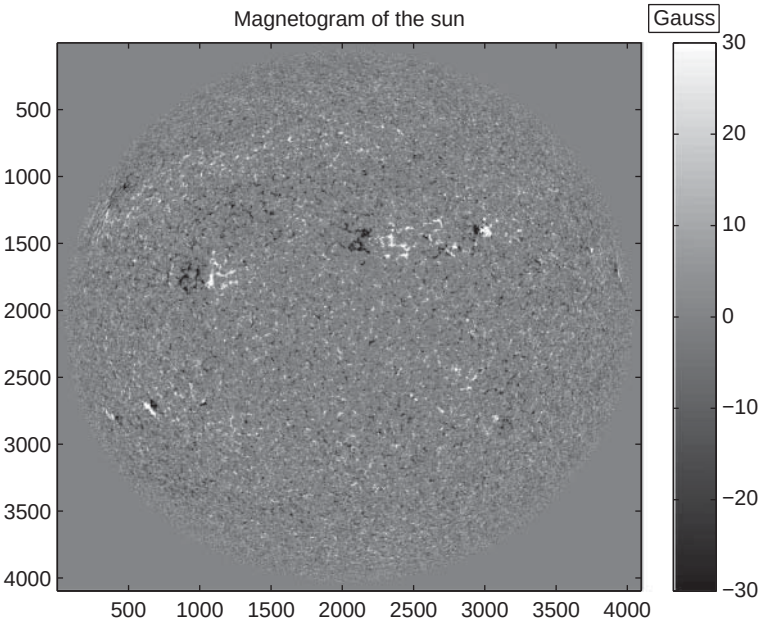

Figure 4. Magnetogram from HMI instrument for the same time of the images in Figure 3.

of the magnetic field. This is because, when there is a large vertical magnetic field, there can be a reconnection event that converts magnetic energy to thermal energy, which would give rise to radiation emission. Thus, the procedure is to locate those regions with high enough brightness coincident with a 'large' magnetic field. To analyze the data we select the emissions according to the scale length and the intensity, and look for correlations with the magnetic field. In projecting the photospheric field up to the corona there is a displacement due to the sun's curvature which increases as one approaches the solar limb. Thus, to minimize projection errors we consider only the central section of the disk delimited by the radius $r = 0.5R_{\odot}$. The range of scale-lengths considered is from 2 to 30 pixels (880–13,200 km). For each scale length l, the procedure to select a region as a reconnection event is the following:

(1) The emission range is restricted to $[I_{\text{av}}, I_{\text{max}}]$ where I_{av} is the average emission within the circle of radius $r = 0.5R_{\odot}$ and I_{max} is the maximum emission recorded in that circle. For 171 Å, $I_{\text{av}} = 300$ counts, $I_{\text{max}} = 2000$ counts, while for 355 Å, $I_{\text{av}} = 4$ counts, $I_{\text{max}} = 600$ counts.
(2) A mean emission I is computed for the square of side l being considered and for the four equal-size adjacent squares; then if the mean emission in any of the adjacent squares is less than that in the central one, this region is included as a candidate event.
(3) At the same location and scale of a candidate event, the magnetic field is examined from the HMI map and if its value B_l is larger than the average value $\bar{B}$ over the whole disk, it is then counted as a reconnection event.

Regarding step (ii), it should be mentioned that this criterion was adopted so that not only isolated events (bright spot surrounded by darker areas all around) are counted, which are rare, but also events with neighbors next to them. There is some chance for counting small-scale events also in larger-scale counts, especially in zones with intricate structure of bright and dark spots. We assume this effect is indeed indicative of the presence of events of different sizes occurring in the same zone, possibly at different heights.

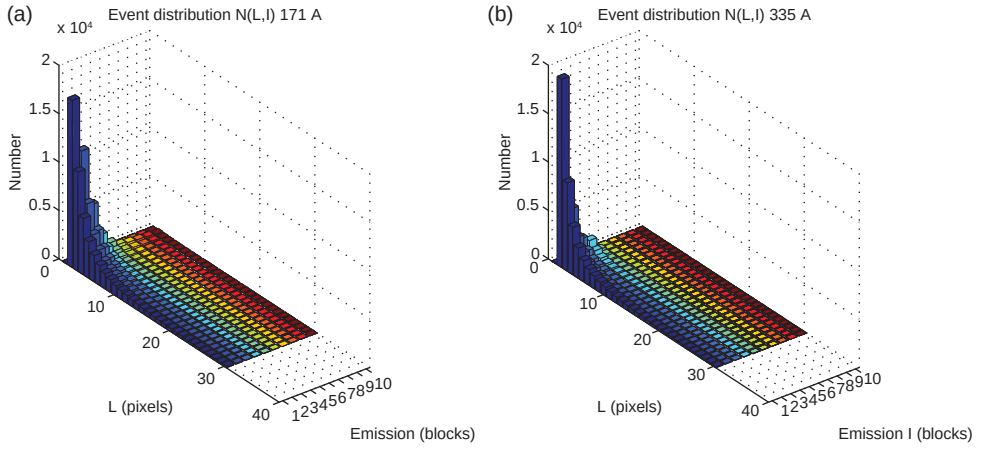

Figure 5. (a) Histogram of reconnection events for 17.1 nm. (b) Histogram of reconnection events for 33.5 nm.

Following this procedure we find a distribution of events $N(l, I)$ as a function of the length l and the intensity I. It contains, for each l, the number of events satisfying the previous criteria grouped according to their emission intensities I. For I, a logarithmic scale is used divided in 10 intervals (or blocks). This procedure is followed for the two observational wavelengths and the resulting distributions of events are shown in Figure 5(a) and 5(b). The two distributions are quite similar as one would expect, with a large contribution from low emissions and small lengths.

4. Heating estimate

Using the event selection obtained from the observational data and the reconnection rates computed in Section 2 we construct a model to estimate the energy released to the corona by all reconnection events on all scales. As a first approximation to the released energy we assume that all the magnetic energy contained in the fields of a given region is converted into free energy. This will give an upper limit for the heating power. We will assume that each region of scale-length l occupies a shallow volume of size $l \times l$ with a depth of one pixel $l_p = 440$ km (the minimum available length). The reason is that the reconnection takes place in current sheets and thus we associate the small width with the depth of the region, which is taken as the smallest available scale (although the actual orientation of the current sheet is arbitrary). Then the volume is $V = l^2 \cdot l_p = l_p^3 n_l^2$, where we take $l = l_p n_l$ denoting by n_l the number of pixels (it runs from 1 to 30). If a volume with larger depth were taken the magnetic energy computed below would be quite larger, so our estimate will give a conservative value. The magnetic energy contained in that region is $W_B = VB_c(l)^2/8\pi$, in terms of the magnitude of the coronal magnetic field $B_c(l)$ for a given scale length l. This is first computed as the mean field over the region of size $l \times l$, but a second estimate will be made using the maximum value within each region. Recall that the coronal field is related with the photospheric field $B(l)$ by $B_c(l) = 0.04B(l)$ (cf. Section 3) which in turn is obtained from the HMI magnetogram for the same region of scale-length l. From the normalized reconnection rate of Figure 2, the reconnection time can be obtained as $t_r = \tau_A/\dot{\hat{\psi}} = \dot{\hat{\psi}}\delta\sqrt{4\pi\rho}/B_c$. The average power at a given scale is then, $P_l = W_B/t_r = [B_c^3/(8\pi) \cdot V\dot{\hat{\psi}}]/(\delta\sqrt{4\pi\rho}) = 1.06 \times 10^{16}\dot{\hat{\psi}}B(l)^3 n_l(l/\delta)$, for an average coronal density of 10^{10} cm^{-3} and B in gauss (G). This is written in terms of the current sheet length-to-width ratio l/δ which is assumed to be the same for all scale lengths. It cannot be known a priori and is treated as a free parameter. The total energy flux released to the corona is obtained

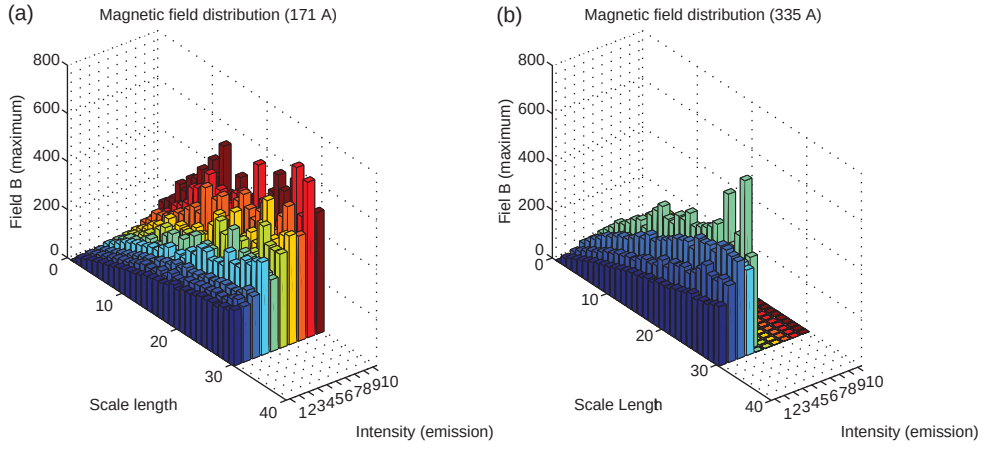

Figure 6. Values of the photospheric magnetic field averaged over the regions with same length and intensity using the data for (a) 17.1 nm and (b) 33.5 nm.

from the sum over all events of the individual powers, divided by the total surface area of the spherical section of projected radius $0.5R_\odot$ that has been considered, that is, $A = \pi R_\odot^2(2-\sqrt{3})$

$$P_B = \frac{\sum P_l}{A} = 2.6\times 10^{-6}\dot{\hat{\psi}}\,\frac{l}{\delta}\sum_{n_l=2}^{30}\sum_{I} B(l,I)^3 N(l,I) n_l \frac{\text{erg}}{\text{cm}^2\text{sec}}. \tag{5}$$

The second equality is an equivalent way of obtaining the energy flux in terms of the event distribution $N(l,I)$. In this expression, the magnetic field $B(l,I)$ represents the average of all the regions corresponding to a given size, l and intensity, I. This average distribution depends greatly on the method for assigning a magnetic field to a region: whether it is the mean value over the region or the maximum value. The one that gives more reasonable results is when the maximum values are used which would represent the one leading to reconnection. This case is presented in Figure 6 for both wavelengths. One can notice the good correlation between high intensity and high magnetic field, which gives support to our hypothesis of identifying bright regions with reconnection events. There is also a good correlation with scale length meaning that larger regions have stronger magnetic fields when reconnection is involved.

Although the properties of the $B(l,I)$ distribution are illustrative, it is not used in our calculations since we adopted the first equality in Equation (5), that is, for each individual event its actual B-field was taken before adding up all the powers.

Now, using Equation (5), the value of the reconnection rate $\dot{\hat{\psi}}$ depends on whether the plasma is collisional or collisionless, yielding different released powers. First the case of only collisional reconnection is considered. When the magnetic field in a region is the mean over that region, the results for the two wavelengths are $P_{B_{171}} = 206(l/\delta)\,\text{erg}\,\text{cm}^{-2}\,\text{s}^{-1}$ and $P_{B_{335}} = 241(l/\delta)\,\text{erg}\,\text{cm}^{-2}\,\text{s}^{-1}$. On the other hand, when the maximum magnetic field in a region is used, the corresponding results for the power released are: $P_{B_{171}} = 1.43\times 10^3(l/\delta)\,\text{erg}\,\text{cm}^{-2}\,\text{s}^{-1}$ and $P_{B_{335}} = 1.4\times 10^3(l/\delta)\,\text{erg}\,\text{cm}^{-2}\,\text{s}^{-1}$. In computing the later, the volume for the magnetic field was taken equal to one cubic pixel since that is the volume corresponding to the maximum field (it amounts to dropping n_l in Equation (5)). The fact that the powers for both wavelengths are quite close indicates a consistency of the method. To get an estimate for the power, it is necessary to have an estimation of the ratio l/δ.

4.1. *Estimate of energy flux within the current sheet*

Another estimate is obtained considering the energy generated by the electric field induced by the reconnection $E = -\partial\psi/c\partial t$. The electric field accelerates particles of charge e and density n in the reconnection region and they are fed energy at a rate determined by the input velocity, v, of the plasma into this region. To compute the power given to the particles let us first consider the energy density given to particles crossing a region of length l, $W = neEl$; during steady reconnection this energy is fed at a rate related to the reconnection time $t_r = t_A/\dot{\hat{\psi}}$, so that the power density is $p_l = neEl/t_r = neEl\dot{\hat{\psi}}/t_A = nelB\delta\dot{\hat{\psi}}^2/(ct_A^2)$, taking the normalization $\psi \sim B\delta$. Hence the power is $p_l = (eB_c^3/c4\pi m_H)(l/\delta)\dot{\hat{\psi}}^2$ (m_H is the hydrogen mass). Since the electric field is confined to the current sheet, the actual volume affected in a scale l is δ/l times smaller than the total volume. Thus, the total released energy flux from the current sheets (CS) is found to be

$$P_{CS} = \sum_I \sum_l \frac{(\dot{\hat{\psi}})^2}{c} \frac{eB_c^3 N(l,I)}{4\pi m_H} \frac{l_p^3}{A} n_l^2. \tag{6}$$

This power input for a collisional plasma using the mean field in each region for the two wavelengths is found to be $P_{171} = (\delta/l)^2 \cdot (3.7 \times 10^5)\,\mathrm{erg\,cm^{-2}\,s^{-1}}$ and $P_{335} = (\delta/l)^2 \cdot (4.37 \times 10^5)\,\mathrm{erg\,cm^{-2}\,s^{-1}}$. These values are of the right magnitude to explain the observations. Now, since these values have to be smaller than those found before, one can obtain an upper bound for the current sheet length ratio, which is $\delta/l \leq 5.5 \times 10^{-4}$. This limit is certainly larger than the very small values usually expected from a Sweet-Parker current sheet of the order of $\delta/l \leq 10^{-5}$ (*14*).

The values quoted above were for the collisional plasma, which are applicable to large scales ($L > \lambda_c$), but for small enough scales (for which $L < \lambda_c$) the plasma is collisionless. Thus, a better estimate of the heating rate is found doing a separation of scales using the corresponding reconnection rate for each regime. It turns out that the transition scale length is 7 pixels. The combined energy flux, including the relative contributions for resistive and non-collisional plasmas, obtained from Equation (6), can be written as

$$P_{CS} = \frac{el_p^3(0.04)^3}{c4\pi m_H A} \sum_I \left[\sum_{n_l=2}^{7} (\dot{\hat{\psi}}_{nc})^2 B(l,I)^3 N(l,I) n_l^2 + \sum_{n_l=8}^{30} (\dot{\hat{\psi}}_c)^2 B(l,I)^3 N(l,I) n_l^2 \right]. \tag{7}$$

The resulting powers, using the mean values of the magnetic field per region are $P'_{171} = 2.4 \times 10^5\,(\mathrm{erg/cm^2\,s})$ and $P'_{335} = 2.8 \times 10^5\,(\mathrm{erg/cm^2\,s})$. For comparison, when the maximum field in each region is used, the power flux for the two wavelengths is $P'_{171} = 4.5 \times 10^5\,(\mathrm{erg/cm^2\,s})$ and $P'_{335} = 4.34 \times 10^5\,(\mathrm{erg/cm^2\,s})$.

These energy fluxes have to be compared with the required flux to maintain the hot corona in the quiet sun, which is $P = 3 \times 10^5\,\mathrm{erg/cm^2\,s}$. The figures from the first computation are somewhat smaller than this value, whereas the estimates with the maximum fields are more in agreement with the observational power. It is then possible that the small discrepancies are due to a missing contribution which can come from smaller scales and intensities than those provided by the *AIA* resolution. These are contributions from nanoflares that are below the resolution limit, which will be considered in the next section.

4.2. *Inclusion of nano-flare scales*

In order to take into account the nano-flare contribution and all the smaller scales, we first obtain the scaling law of $N(I,l)$ from the observations presented in Figure 5 and then use it

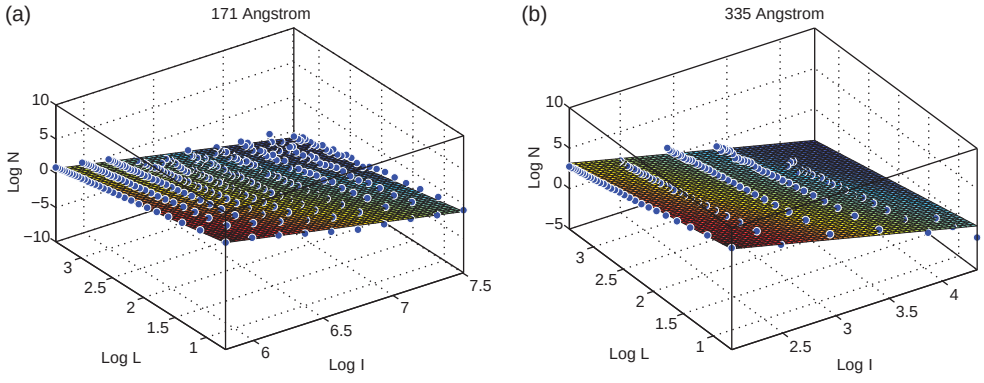

Figure 7. (a) Regression surfaces in log–log scale for the best fit to the distribution of events for the wavelengths (a) 17.1 nm and (b) 33.5 nm. The dots represent the data. (a) Fit to distribution for 171 Å, (b) fit to distribution for 335 Å.

to extrapolate to lower scales. Assuming a power law dependence

$$N(n_l, I) = K n_l^{\alpha} I^{\beta}, \tag{8}$$

we find that the best fit to the data for the wavelength 171 Å has $K = 6.4 \times 10^{12}$, $\alpha = -1.78$, $\beta = -3.92$ with confidence intervals $[3.59,\ 11.46] \times 10^{12}$; $[-1.85,\ -1.72]$; $[-4.007,\ -3.84]$, respectively. For the wavelength 335 Å the coefficients are $K = 2.5 \times 10^6$, $\alpha = -1.6$, $\beta = -3.05$ with the respective confidence intervals $[1.38,\ 4.5] \times 10^6$; $[-1.727,\ -1.464]$; $[-3.185,\ -2.905]$. The power law fits for the two cases are presented in Figure 7 in the log–log scale showing good agreement with the data. Analogous dependencies were found by Porter and Klimchuk (*15*) from observations with Yohkoh for the heating rate, obtaining $\sim l^{-2} \sim n_l^{-2}$. Also, the scalings with the length, n_l, are within the range $1 \leq \alpha \leq 2$ found by Mandrini et al. (*2*) for all the coronal heating models analyzed based on DC processes. Thus, our scalings are consistent with previous studies.

With these scalings we can extend the calculations to include scales and intensities below the resolution and sensibility limits of the instruments. We concentrate here on the computations using the mean magnetic field in the different scales since that is the one that produces heating powers smaller than those required. The energy flux is computed using the same expressions found before (Equation (7)) but keeping only the contribution for collisionless reconnection, since that is the relevant one for the extrapolated small scales. In this case the sums are replaced by integrals over the intensities and length scales, with the lower limits extended to the required values. In this way we can determine whether or not the small scales can contribute to account for the needed energy flux and if so, determine the smallest scales that have to be to included.

For the event distribution scaling in Equation (8) the total energy flux, including the contribution for scales below 1 pixel, would take the following form:

$$P_{\mathrm{Tot}} = \frac{e(0.04 l_{\mathrm{p}})^3 K}{4\pi c m_{\mathrm{H}} A} \int_{I_0}^{I_{\max}} \mathrm{d}I \int_{n_0}^{1} \mathrm{d}n_l (\dot{\hat{\psi}}_{\mathrm{nc}})^2 B^3 I^{\beta} n_l^{\alpha+2} + P_{\mathrm{CS}}, \tag{9}$$

where n_0 and I_0 are the smallest scales contributing to the heating and P_{CS} is the flux already computed in Equation (7). The value of B at these scales is not known but we can use the result found by Mandrini et al. (*2*) for the scaling $B(l)$, giving that for small scales there is no dependence on l (*i.e.* $B \propto l^0$). Then B^3 can be taken as a constant and equal to the average photospheric value $B = \bar{B} = 6.9$ G. Equation (9) can be used to find the conditions on the lower limits n_0 and I_0 required to match the observed coronal energy flux: making $P_{\mathrm{Tot}} = 3 \times 10^5$ erg/cm^2 s and taking the values of P_{CS} found above.

One important result is that, since the exponent $\alpha > -2$, the integrand in n_l is an increasing function and therefore the integral for $n_l \leq 1$ does not contribute substantially to the energy flux. The important contribution comes from the I scaling which is a deceasing function ($\beta < 0$), and its integral can be quite large if I_0 is small enough. Thus, the very numerous low-emitting regions could provide the necessary power. From the calculations we find that, for 171 Å the minimum intensity needed is $I_0 = 16.5$ counts, whereas for 335 Å the minimum intensity has to be close to zero ($I_0 = 0.08$), thus, practically all existing events are required. This also implies that energy release from emission at 17.1 nm is more efficient in heating. These results would be valid provided the scaling of Equation (8) is still applicable for the lowest intensities and lengths.

5. Discussion and conclusions

The study presented here aims to have an overall estimate of the energy flux into the corona provided by reconnection events at all scales, in order to contribute to answer the question of what is the source of coronal heating. This is a complex problem, which we are simplifying substantially so that a workable solution can be given. Many assumptions are made, some more questionable than others, but within that framework we provide certain values for the energy flux that can be compared with the actual required value of $300\,\mathrm{W/m^2}$. The evaluations are divided into two parts: first, we used a reconnection model to determine the reconnection rates in both a resistive plasma and a collisionless plasma; then an accounting of reconnection events is made based on observations using specific criteria. Combining the two parts, a computation of the total energy released to the corona per unit time and unit area is performed. The crucial question is how to identify reconnection events observationally and for this we assume that the emitting regions in the corona which cover a finite region (of length l) which coincide with a large enough magnetic field can be selected as such. This can be justified by arguing that the presence of large enough fields may lead to reconnection, when current sheets are created, and the released energy is radiatively emitted. Assuming that these processes occur continuously in the corona, an average value for the heating power can be obtained from an image of the corona at any time.

Based on the assumptions, a distribution of reconnection events was found for two emission wavelengths, corresponding to active corona and quiet corona (and transition region), as a function of scale-length and intensity. This was first used to find an upper limit to the heating rate, by assuming all magnetic energies in the reconnection regions are converted to heat, through resistive reconnection, which turns out to be a function of the current sheet aspect ratio, δ/l. A more realistic evaluation was made based on the energy transferred by the electric field created in the reconnection current sheet. Since δ/l is not known a priori, it was possible to find an upper limit for this by comparing the heating power to its upper limit found before. A further improvement of the computations was found when the reconnection process is separated in collisional, for large scales, and collisionless, for small scales. In that case the upper limit for δ/l was used, so this too provides an upper limit for the total energy flux. Since theoretical models suggest the value of δ/l is smaller than the limit, it is likely that the heating power is quite smaller than the one found here.

Two ways of assigning a value of the magnetic field to the different scale regions were used. The more conservative one takes the mean value over the relevant region but this underestimates the fields that are concentrated in small areas, which are mainly responsible of reconnection. Thus, in a second estimate the maximum magnetic field is taken and the corresponding area is reduced to the resolution limit. The upper limit of the energy flux (given by the full conversion of magnetic energy) obtained for the mean field is six to seven times smaller than the flux for the maximum field. However, the values for the more realistic model differ only by less than a factor

of two; the difference is less for the long wavelength (335 Å, active corona) meaning the field determination is less important for the active corona. The largest limit values are of the order of the required $300\,\mathrm{W/m^2}$ flux, thus the actual flux would be smaller than this.

The fact that our estimates are under the expected value, led us to suggest that the contribution of events below the resolution and sensitivity limits of the instruments should be important. The relevance of this hypothesis was tested by first finding a power-law fit to the distribution function $N(l, I)$ and then using it to extrapolate the heating to smaller scales and dimmer intensities. The extremely large number of events at low intensities could account for the difference from the needed heating power. In contrast, the scale-length scaling does not have a steep enough variation (*i.e.* $\alpha < -2$) to have a significant contribution for small lengths.

In summary, the results found here support the assumption that the magnetic reconnection process can be the main source of coronal heating. From the present analysis it follows that the required energy flux to the corona can be accounted for by magnetic reconnection events of all length-scales down to the nano-flare scales. This does not mean that this is the only process that contributes since processes like Alfvén wave heating can also be present. Actually, the most likely situation is that more than one process takes place simultaneously, although the DC mechanisms in multiscales could be enough.

Acknowledgments

This work was supported by projects DGAPA-UNAM IN106911 and CONACyT 152905.

References

(1) Klimchuk J.A. *Solar Phys.* **2006**, *234*, 41–77.
(2) Mandrini C.H.; Démoulin P.; Klimchuk J.A. *Astrophys. J.* **2000**, *530*, 999–1015.
(3) McIntosh S.W.; DePontieu B.; Carlsson M.; Hansteen V.; Boerner P.; Goossens M. *Nature* **2011**, *475*, 477–480.
(4) Tomczyl S.; McIntosh S.W.; Keil S.L.; Judge P.G.; Schad T.; Seeley D.H.; Edmondson J. *Science* **2007**, *317*, 1192–1196.
(5) Parker E. *Astrophys. J.* **1988**, *330*, 474–479.
(6) Su Y.; Veronig A.M.; Holman G.D.; Dennis B.R.; Wang T.; Temmer M.; Gan W. *Nature Phys.* **2013**, *9*, 489–493.
(7) Delzanno G.L.; Fable E.; Porcelli F. *Phys. Plasmas* **2004**, *11*, 5212–5228.
(8) Kuvshinov B.N.; Lakhin V.P.; Pegoraro F.; Schep T.J. *J. Plasma Phys.* **1998**, *59*, 727–736.
(9) Martinell J.J. *Rad. Effects Defec. Solids* **2010**, *165*, 114–122.
(10) Bogod B.M.; Yasnov L.Y. In *Universal Heliophysical Processes*; Gopalswamy, N., Webb, D.F., Eds.; IAU Symposium 257; Cambridge University Press: UK, 2009; pp 349.
(11) Cho K.-S.; Lee J.; Gary D.E.; Moon Y.-J.; Park Y.D. *AstroPhys. J.* **2007**, *665*, 799–804.
(12) Dulk G.A.; McLean D.J. *Solar Phys.* **1978**, *57*, 279–295.
(13) Robertson J.A.; Hood A.W.; Lothian R.M. *Solar Phys.* **1992**, *137*, 273–292.
(14) Aschwanden M.J. *Astrophys. J.* **2008**, *672*, L135–L138.
(15) Porter L.J.; Klimchuk J.A. *Astrophys. J.* **1995**, *454*, 499–511.